

# Data-Adaptive Autonomous Seakeeping

Michael D. Levine<sup>1</sup>, Samuel J. Edwards<sup>1</sup>, Dayne Howard<sup>2</sup>,

Vadim Belenky<sup>1</sup>, Kenneth Weems<sup>1</sup>, Themistoklis Sapsis<sup>2</sup>, and Vladis Pipiras<sup>3</sup>

<sup>1</sup>Naval Surface Warfare Center, Carderock Division

<sup>2</sup>Massachusetts Institute of Technology, <sup>3</sup>University of North Carolina

## ABSTRACT

The safe operation of a ship in heavy weather and high sea states requires accounting for the risk of extreme ship motion responses in stochastic ocean waves. Excessive ship motions can lead to hazardous and unsafe conditions such as pure loss of stability, surf-riding and broaching. Mitigation of these risks is typically performed through selection of ship headings and speeds for the given seaway, and avoiding conditions likely to lead to severe motions. To address this challenge, a robust, onboard, fast data-adaptive model is needed to evaluate the expected ship motion responses to the ocean environment, and ship loading conditions. In this study, data-adaptive Long Short-Term Memory (LSTM) neural networks are investigated as part of a multi-fidelity approach incorporating Large Amplitude Program (LAMP), and a reduced-order model known as SimpleCode. An initial assessment of this multi-fidelity approach has focused on prediction of ship motion responses in waves. LSTM networks were trained and tested using LAMP simulations as a target, and SimpleCode simulations and wave time-series as inputs. LSTM networks were shown to improve the fidelity of SimpleCode seakeeping predictions relative to LAMP while retaining the computational efficiency of a reduced-order model. Potential areas of application for data-adaptive autonomous seakeeping include unmanned and reduced crewed vessels, as well as operator guidance for manned systems.

## 1. BACKGROUND AND INTRODUCTION

To ensure the safe operation of a ship in heavy weather conditions, operational guidance attempts to mitigate

the risk of severe motion events by selecting ship headings and speeds that minimize the probability of stability failures in the encountered wave conditions. This mitigation requires a reliable assessment of the seakeeping response of the hull with consideration of the loading conditions.

Due to the inherently random character of the maritime environment, not all dangerous situations can be addressed and prevented at the design stage. The 1998 stability accident involving APL (American President Lines) China experiencing parametric roll resonance (France et al. 2003) highlighted the need for ship-specific operational guidance; since parametric roll could not be prevented with reasonable design measures (Shin et al. 2004). An important implication of the APL China accident is that a ship cannot be made safe solely by design. No meaningful design changes can readily prevent parametric roll (Levadou and van't Veer, 2006). Consequently, this real-world example highlights the importance of providing seakeeping guidance during ship operations.

Operational guidance has been a subject of ongoing technical consideration. One of the first recommendations on avoidance of dangerous situations was published by the Maritime Safety Committee (MSC) of International Maritime Organization (IMO) MSC/Circ. 707 in 1995. Superseded by MSC/Circ. 1228 in 2007, it offered general recommendations without consideration of ship-specific behavior.

Recently, ship-specific operational guidance became a part of the IMO Second Generation Intact Stability Criteria, which addressed pure loss of

stability, parametric roll, excessive accelerations, and surf-riding boarding modes of stability failure (MSC.1/Circ. 1627). Operational guidance is expected to be developed through state-of-the-art ship motion numerical simulation procedures. The main intent of operational guidance is to inform the crew of specific features and behaviors of a ship, and aid in making informed decisions concerning ship operations in severe weather. The development of operational guidance for unmanned or reduced-crew vessels further expands the technical scope of the problem.

Development of seakeeping guidance typically entails generation of a lookup table of responses for pre-defined wave and loading conditions. From the lookup table, the expected ship response is extracted corresponding to the encountered or forecasted sea conditions.

Applicable seaway parameters available from weather forecasts include:

- Significant wave height of primary system
- Modal (or mean-zero crossing) period of primary system
- Spread for primary system
- Significant wave height of secondary system
- Modal period of secondary system
- Spread for secondary system
- Propagation angle between the primary and secondary systems.

In addition to the environment, the generation of the lookup table requires information on loading conditions including draft, vertical location of the center of gravity (KG), and trim.

Considering these parameters, the resultant lookup table has 10 dimensions. The problem of interpolation of a high dimensional parameter space is non-trivial. Consequently, the number of parameters needs to be decreased when developing pre-computed operational guidance. Dimensionality may be reduced based on correlation analysis and approximation of the wave parameter space (Levine et al., 2021).

Physics-based hydrodynamic models for seakeeping are well-established (Lin and Yue, 1990; Beck and Reed, 2001; Shin et al. (2003); Reed and Beck (2016); Belknap and Reed, 2019. Most practical nonlinear seakeeping models employ a hybrid approach encompassing potential flow hydrodynamics with empirical coefficients, which are derived from model test data, high fidelity computational fluid dynamics (CFD), or engineering guidelines. While significantly faster than CFD, these hybrid models still

require significant computational resources that preclude real-time processing.

## 2. APPROACH

To address the challenge of onboard autonomous seakeeping, a data-adaptive multi-fidelity approach may provide a plausible way for evaluating the expected ship motion responses for given seaways and ship loading conditions. Such a model could provide actionable information for autonomous seakeeping to improve safety of operation in realistic environments.

In Levine et al. (2021), a reduced-order model known as SimpleCode was introduced as a potential candidate for automated seakeeping guidance. SimpleCode employs a volume-based algorithm that models the body-nonlinear hydrostatic and Froude-Krylov forces. The resulting code is very fast, and able to produce hundreds of hours of responses in a matter of seconds (Weems and Wundrow, 2013).

While this reduced-order model offers a significant advantage in processing speed, a fidelity gap still exists in the estimation of nonlinear responses as compared to predictions from a higher-fidelity but computationally intensive model such as Large Amplitude Motion Program (LAMP) in Shin et al. (2003).

In this paper, Long Short-Term Memory (LSTM) neural networks are considered as part of a multi-fidelity approach for the prediction of 3-DOF (heave, roll and pitch) ship motion responses in waves. LSTM networks are trained and tested using LAMP simulations as a target, and SimpleCode simulations and wave time-series as inputs. Simulations are performed based on a model of the ONR Tumblehome. In this initial feasibility study, LSTM networks are assessed in terms of improving the fidelity of SimpleCode seakeeping predictions relative to LAMP, while retaining the computational efficiency of a reduced-order model.

The following sections provide the technical framework for realization and assessment of this multi-fidelity approach.

### 2.1 Reduced-Order Simulations

The main idea of SimpleCode is that by simplifying the local variation of wave pressure (i.e. Smith effect in Bertram, 2011), the surface integral can be converted to a volume integral in the equations for hydrostatic and Froude-Krylov forces by employing

Gauss theorem (equations 1 through 13 in Weems and Wundrow, 2013).

As a result, the sectional hydrostatic and Froude-Krylov forces need only evaluate the instantaneous submerged volume and its geometric center. These calculations can be implemented to run quickly with pre-computed Bonjean curves for each station plus a triangle correction reflecting the instantaneous roll relative to the wave as shown in Figure 1. The sectional calculation requires:

- Finding an intersection of flat waterline with sides
- Interpolation of pre-computed Bonjean curve in two points
- Calculation of correction values for area and moments as shown in light blue in Figure 1.

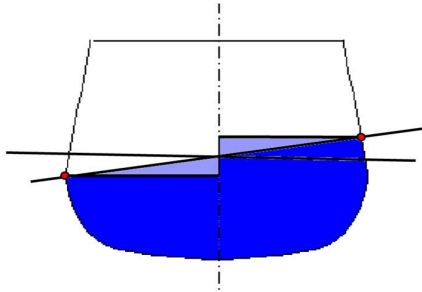


**Figure 1:** Sample sectional volume calculation for the ONR Topsides Series Tumblehome hull.

The complete instantaneous submerged volume and its center is computed by integration of sectional values over the hull shown in Figure 2.

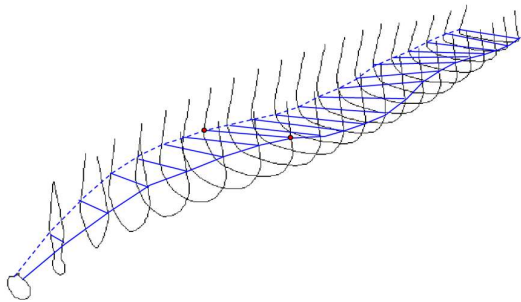


**Figure 2:** Station and incident wave intersection points for ONR Tumblehome hull in stern oblique seas.

The original application of SimpleCode was for statistical validation of extrapolation methods (Smith, 2019), where the only requirement was qualitative validity. This qualitative validity was assured through reproduction of the inseparability of the hydrostatic

and Froude-Krylov forces, which are understood to contribute significantly to the nonlinear characteristics of ship dynamics in waves.

As described in Weems and Belenky (2018), SimpleCode can produce a reduced-fidelity approximation based on comparisons with LAMP even with diffraction and radiation forces turned off. Recent development shows that diffraction and forces may be estimated in the SimpleCode through coefficients derived by regression techniques (Pipiras et al. 2021), with no significant impact on computational speed.

Another relevant development has focused on maneuvering forces and motions in the horizontal plane. Weems et al. (2020) describe an implementation of maneuvering hull forces based on regression from simplified Reynolds Averaged Navier-Stokes (RANS) simulations (double body – drift and rotating arm test). Employing regression for estimating hydrodynamic derivatives is a well-established technique, and results are applicable to SimpleCode.

Radiation forces in SimpleCode can be captured through a set of added mass and damping coefficients. These coefficients can be tuned to LAMP by a physics-informed approach suggested in Pipiras et al. (2021, 2022). Forced LAMP runs can yield hydrodynamic forces consisting of radiation forces, which are then regressed on motion accelerations and velocities. Diffraction forces can be incorporated as additional forcing into SimpleCode through another set of frequency dependent coefficients that are now obtained through penalized regression of the hydrodynamic forces from the fixed-body LAMP calculation. Pipiras et al. (2021, 2022) show the feasibility of these methods, but their full integration and testing in SimpleCode is still ongoing.

Assessment of uncertainty is an important consideration in operational guidance. Weems et al. (2020) describe how uncertainty is evaluated for regression-based hydrodynamic derivatives and can be applied throughout the equations of motions. Levine et al. (2017) present statistical uncertainty techniques for analysis of seakeeping data.

As a result, current SimpleCode appears suitable as a reduced-fidelity simulation tool, which combines volume-based calculations for hydrostatic and Froude-Krylov with regression-based diffraction, radiation and maneuvering forces. This reduced-fidelity model

may include uncertainty quantification, making it a potentially viable approach for computationally efficient predictions of six degree of freedom (6-DOF) motion responses of a hull form for a defined set of wave conditions.

## 2.2 Long Short-Term Memory

An LSTM network (Hochreiter and Schmidhuber, 1997) is a type of recurrent neural network, which incorporates both short and long-term effects based on data-adaptive learning for estimation of a system, function, or process. The architecture of an LSTM cell is shown in Figure 3.

Inside the cell, the circled functions labeled  $(f_1, f_2, f_3, f_4)$  are representative of an LSTM unit, and circled operators are component-based operations. *Sigma* ( $\sigma$ ) is the sigmoid activation function, and *tanh* is the hyperbolic tangent activation. The size of the weight and bias matrices in the LSTM unit defines the size or dimensionality of the hidden state and cell state.

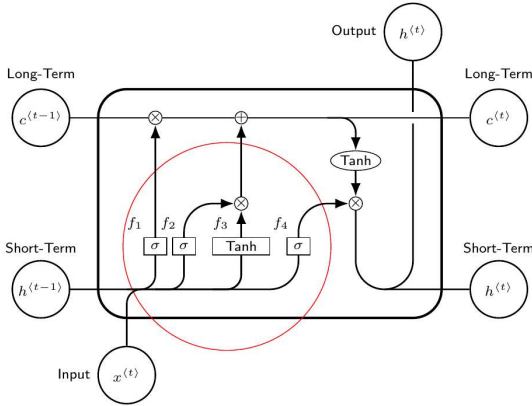


**Figure 3:** Basic architecture of an LSTM cell including the inputs, outputs, and short and long-term memory components.

The following equations show the compact form of the operations inside of the cell.

$$f_1 = \sigma(W_{f_1} \cdot x^{(t)} + U_{f_1} \cdot h^{(t-1)} + b_{f_1}) \quad (1)$$

$$f_2 = \sigma(W_{f_2} \cdot x^{(t)} + U_{f_2} \cdot h^{(t-1)} + b_{f_2}) \quad (2)$$

$$f_3 = \tanh(W_{f_3} \cdot x^{(t)} + U_{f_3} \cdot h^{(t-1)} + b_{f_3}) \quad (3)$$

$$f_4 = \sigma(W_{f_4} \cdot x^{(t)} + U_{f_4} \cdot h^{(t-1)} + b_{f_4}) \quad (4)$$

$$c_t = f_1 \circ c^{(t-1)} + f_2 \circ f_3 \quad (5)$$

$$h_t = f_4 \circ \tanh(c^{(t)}) \quad (6)$$

Weights are represented by  $(W, U)$ , biases  $(b)$ , and Hadamard product ( $\circ$ ). Each of the weights and biases are “learned” based on the training of the neural network. The hidden state  $(h_t)$  and cell state  $(c_t)$  are what change through time and act as “memory”.

Function  $(f_1)$  is the “forget gate” that controls the parts of the long-term state that are deleted. Function  $(f_3)$  represents the input gate, which controls the information from  $(f_2)$  that is added to the long-term state. The function  $(f_4)$  controls the output gate, which determines the output of the long-term state.

By constructing layers of cells, the LSTM network is capable of forecasting a desired response to the given relevant input. An LSTM network effectively maps the input time-series to the desired output time-series or target(s). Adding more units to each cell or increasing the number of layers can enable the network to model more complex interactions or behaviors.

The training process for the LSTM network is dependent on the selection of a number of hyperparameters. The accuracy and time-efficiency of an LSTM network depend on the hyperparameters.

The hyperparameters are comprised of the number of inputs, number of network layers, training data sequence length, time resolution of input time-series, hidden state size, bi-directionality, and dropout method. The length of the training data sequences is equivalent to the number of samples of the input time-series.

Time resolution is based on uniform resampling of the input and target time-series. By resampling, each time-series is reconfigured into a matrix of size  $[N/\tau, \tau]$ ; where,  $N$  is the original time-series length, and  $\tau$  is the time resolution factor. If  $N$  is not divisible by  $\tau$ , then the time-series is reduced in length to the closest multiple of  $\tau$ .

The network includes layers of LSTM cells that contain the hidden states. The hidden state size is the number of parameters  $(h_t)$ , which affects the number of weights in an LSTM unit. Size of the weights vectors are  $W \in R^{h \times d}$  and  $U \in R^{h \times d}$  for hidden state size  $(h)$ , and number of input time-series channels  $(d)$ .

Increasing the hidden state size and number of LSTM layers can improve the ability of the network to recognize patterns with greater complexity, but can also result in model over-fitting and increased training time.

Bi-directional networks consider the relationship between input and target time-series for both forward

and backward directions in time. Incorporation of bi-directionality generally increases the number of patterns that can be recognized, but results in longer training times.

Dropout is a regularization method where the individual units and their corresponding connections are removed temporarily from the network on a random basis of probability ( $p$ ). This random removal during training enables reduction in over-fitting. During testing, the units and connections are restored and trained, with weights ( $w$ ) then becoming the expected weights ( $p \cdot w$ ).

Recent applications of LSTM networks to ship hydrodynamics include the prediction of nonlinear roll in response to irregular waves by Xu et al. (2021); and forecasting and correcting time-series using LSTM networks in Qiao et al. (2021), where ship motion data was an input into an LSTM network to predict mooring line tension time-series.

### 3. METHODOLOGIES AND MODELS

#### 3.1 Overview

Operational guidance is essentially a set of motion responses computed for a range of potential ship speeds and headings for the encountered wave conditions. Based on application of the prescribed limits to ship motions, recommended safe speeds and headings for the seaway can be provided.

The validity of this guidance depends on the accuracy and reliability of these motion response predictions, which are based on the quantitative validity of the simulation system employed. Here, this validity is provided with what is essentially a multi-fidelity approach. The approximations employed in the reduced fidelity models are generated by higher fidelity simulation tools that appear to be quantitatively valid.

Application of this multi-fidelity approach requires additional steps in the development of automated operational guidance, which includes running additional simulations and verifications. The number and complexity of these steps depends on the completeness of the reduced-order model in SimpleCode. Current and prospective methodologies and models for the development of operational guidance are presented in the following sections.

#### 3.2 3-DOF Reduced-Order Model

The 3-DOF reduced-order model includes vertical motions: heave, roll and pitch. Following requirements of the Second Generation Intact Stability

Criteria MSC.1/ Circ. 1627, this model can handle excessive accelerations and parametric roll failure modes. A procedure is envisioned based on the following steps:

1. Estimation of damping, following the updated International Towing Tank Conference (ITTC 2021) Recommended Procedure 7.5-02-07-04.5.
2. Estimation of diffraction and radiation forces for heave, roll and pitch through a series of potential flow simulations and regression following the method in Pipiras et al. (2021).
3. If roll damping is based on model testing or RANS simulations, where the wave component is inherently included, then additional roll damping calibration is needed; based on Section 3.3.2.2 of MSC.1/ Circ. 1627, with more details available from section 6 of Belenky et al. (2011).
4. Select several of the most probable sea states and run potential flow simulation tool for these sea states, with damping calibration results from the previous step. The reduced-order simulation tool is run to verify consistency.

#### 3.3 6-DOF Reduced Order Model

A complete 6-DOF reduced-order model can address surf-riding and broaching failure modes (e.g. Weems et al. 2020) as well as pure loss of stability (MSC.1/ Circ. 1627 recommends use of at least 4-DOF model surge-sway-roll-yaw).

Study of the consistency of multi-fidelity modeling has continued with Pipiras et al. (2021, 2022). The intent of these studies has been to develop procedures and robust reduced-order model for generating approximate quantitatively correct responses.

#### 3.4 Generation of Operational Guidance

Once a weather report is received on board a vessel, expected seaway conditions are known and elevations  $\zeta_w$  of irregular waves can be computed with Longuet-Higgins model. For the case of long-crested waves:

$$\zeta_w(x, t) = \sum_{i=1}^N a_i \cos(k_i x - \omega_i t + \varphi_{0i}) \quad (7)$$

$x$  is a longitudinal coordinate,  $t$  is time,  $a_i$  is an amplitude of the  $i$ -th wave component,  $k_i$  is wave number (spatial frequency) of  $i$ -th wave component,  $\omega_i$  is temporal frequency of  $i$ -th wave component, and  $\varphi_{0i}$  is a random initial phase  $i$ -th wave component; uniform distribution of 0 to  $2\pi$  is assumed for the

random initial phases. The wave number is computed from frequency, where  $g$  is gravity acceleration, using the Airy wave dispersion relationship:

$$k_i = \frac{\omega_i^2}{g} \quad (8)$$

The amplitudes  $a_i$  are computed from spectral density where  $\Delta\omega$  is a frequency increment:

$$a_i = 2\sqrt{s(\omega_i)\Delta\omega} \quad (9)$$

While,  $s(\omega_i)$  is a resultant spectral density:

$$s(\omega_i) = s_I(\omega_i) + s_{II}(\omega_i) \quad (10)$$

where  $s_I$  is the spectral density of the primary wave system (typically wind waves), and  $s_{II}$  is the spectral density of the secondary wave system (swell).

The capability to account for the secondary wave system would be difficult for precomputed operational guidance but is reasonably straightforward with the current approach.

The choice of the frequency set  $\omega_i$  and frequency increment  $\Delta\omega$  requires careful consideration in order to avoid self-repetition, as recommended in paragraph 3.3.2.1.2 of IMO (2020) MSC.1/Circ. 1627; Belenky (2011) for theoretical background. The self-repetition effect compromises the statistical validity of the wave model. To avoid the self-repetition effect, the number of wave components should be sufficient for the selected length of the ship motion record. A record is characterized by a unique set of initial random phases. Increasing the duration of the record requires increasing the number of wave components and leads to an increase in the computational cost of the wave evaluation. A practical approach is to use several shorter records. Thus, a set of records is the outcome of ship motion simulation of a single speed and heading combination for a given seaway.

Conventionally, operational guidance is generated and displayed as a speed-heading polar plot, which is defined by combinations of ordered speeds and wave headings (relative to primary wave system).  $N$  ordered speed increments and  $M$  relative heading increments result in a total of  $N \times M$  speed heading nodes for a plot. A set of motion parameters is computed for each ordered speed-wave heading combination (or node). For a given node, if all the relevant ship motion parameters are less than an established threshold, then the node is designated as

safe. If one or more of the parameters exceed the threshold, then the risk index is designated as unsafe.

Once the polar plot is computed, automated heavy-weather guidance can be applied. Its action is envisioned as part of route planner, which directs the autopilot to avoid certain headings, and imposes speed restrictions.

The choice of the motion parameters is still a somewhat open issue. American Bureau of Shipping (ABS 2019) uses maximum value of roll angle observed during certain time of simulation. MSC.1/Circ. 1627 recommends two alternatives:

1. Upper boundary of the confidence interval for failure rate estimate (for probabilistic guidance, section 4.5.4 of MSC.1/Circ. 1627).
2. Two times the 3-hour maximum roll or lateral acceleration (for deterministic guidance section 4.5.5 of MSC.1/Circ. 1627).

### 3.5 Data-Adaptive Multi-Fidelity Model

An objective of this study is to assess the initial feasibility of data-adaptive ship motion models for autonomous seakeeping. An emerging capability is data-adaptive tuning (or correction) of reduced-order model predictions based on training with higher fidelity ship motions response data. The intent of applying a data-adaptive approach is to improve the fidelity of the prediction. Application of higher fidelity data may also improve validity of reduced-order models.

In this study, the hull form geometry and loading conditions are based on a model of the ONR Tumblehome configuration from the ONR Topsides series (Bishop, et al.). A rendering of the hull for the ONR Tumblehome model is in Figure 4. The particulars are shown in Table 1.

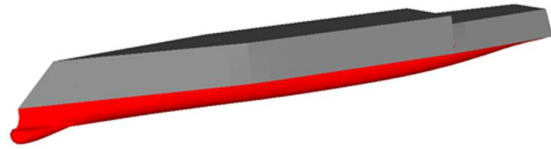


**Figure 4:** Rendering of hull for ONR Tumblehome.

**Table 1:** ONR Tumblehome Particulars

Particular	Symbol	Value
Length	$L_{BP}$	154.0 m
Beam	$B$	22.0 m
Draft	$T$	5.5 m
Displacement	$\Delta$	8730.0 t

In this framework, the higher fidelity target is LAMP and reduced-order model is SimpleCode. For this given hull form geometry, wave conditions, and specified ship speeds and headings, LAMP simulations generate pseudo-random irregular waves and output 3-DOF motion response time-series, which serve as training and testing datasets. The equivalent input wave data are then applied to SimpleCode, which generates reduced-fidelity response time-series.

Two data-adaptive machine learning methods are considered. The first method is referred to as LSMT-Waves, and second as LSTM-SimpleCode. A basic view of architecture of LSTM-Waves and LSTM-SimpleCode methods are shown respectively in Figures 5 and 6.

An additional fully connected linear output layer has been inserted after the two LSTM layers to parse the output into individual time-series channels for the 3-DOF motions in terms of roll, pitch and heave.

Definitions of the hyperparameters are shown in Table 2.

**Table 2:** Parameters for LSTM Architecture

Variable	Definition
$\eta_{0,j}$	Input wave at time-step $j$
$T$	Total number of time steps
$\eta_{i,j}$	$i$ - th degree of freedom at time-step $j$
$f_k$	The $k$ - th gate for the LSTM layer
$n$	Number of LSTM units per layer
$O_m$	Output layer cell for degree of freedom $m$

LSTM-Waves method employs an LSTM network that is directly trained and tested with high-fidelity LAMP data. As such, this LSTM-Wave network is strictly data-driven and not physics-based. The single channel wave time-series are applied as input to the LSTM network. The output response time-series from the LSTM network are compared with the corresponding 3-DOF motion time-series from LAMP. Based on the difference between the LSTM and the target LAMP response outputs, an adaptive learning rule is applied for the adjustment (or tuning) of the LSTM network cells. During testing, the output responses of the trained LSTM-Wave network are compared with high-fidelity LAMP baseline data.

LSTM-SimpleCode method is comprised of two-stages with SimpleCode as the first stage and LSTM network as the second. LSTM-SimpleCode is characterized as a hybrid approach comprised of a physics-based model and data-adaptive stage. In this

architecture, four time-series channels are applied as inputs to the LSTM network. The input channels encompass the 3-DOF motion responses from SimpleCode and the corresponding input wave time-series data. The output response time-series from the two-stage SimpleCode-LSTM scheme are compared to the 3-DOF motion time-series from LAMP.

To assess the performance of the LSTM methods, LAMP and SimpleCode time-series were generated for a set of speed-heading combinations. Ship speeds ranged from 0 to 30 knots in 5 knot increments, and headings from 0 to 180 degrees in 15 degree increments for a total of 91 speed-heading combinations. The model is free in the vertical plane for heave, roll and pitch, but constrained to constant course and speed in the horizontal plane for surge sway and yaw.

The inputs were rearranged into  $[n, N/\tau, \tau]$  arrays by number of inputs ( $n$ ), number of points per realization ( $N$ ), and time resolution factor ( $\tau$ ). Each LSTM layer consists of a single LSTM cell with its own set of gates ( $f_1, f_2, f_3, f_4$ ) and distinct weights and biases.

A total of 30 realizations of LAMP data was generated with different sets of pseudo-random phases to ensure independence between realizations. Each realization was 30 minutes duration and 10 Hz sample rate. The objective function for training was the mean-squared error (MSE) between LAMP and the LSTM output. The equation for MSE is given by:

$$MSE = \frac{1}{N} \sum_{i=1}^N (y_L(t_i) - y_s(t_i))^2 \quad (15)$$

LAMP time-series is represented by  $y_L(t)$ , response time-series (from SimpleCode or LSTM network output as applicable) is represented by  $y_s(t)$ , number of points in time-series ( $N$ ), and time index  $t_i$ .

For training, individual LSTM networks were generated for each of the 91 speed-heading combinations. This was performed for LSTM-Waves and LSTM-SimpleCode networks separately, which resulted in a total of 182 individually trained LSTM network architectures. Alternatively, the LSTM networks could be trained with a more general approach covering a multiple set of speeds and headings. However, this greater generality could lead to reduced fidelity.

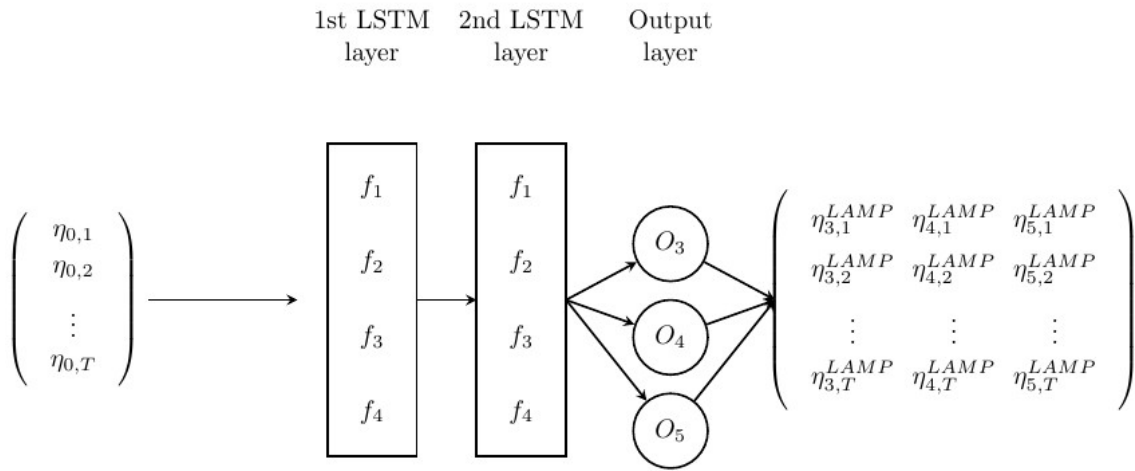


**Figure 5:** LSTM-Waves Architecture

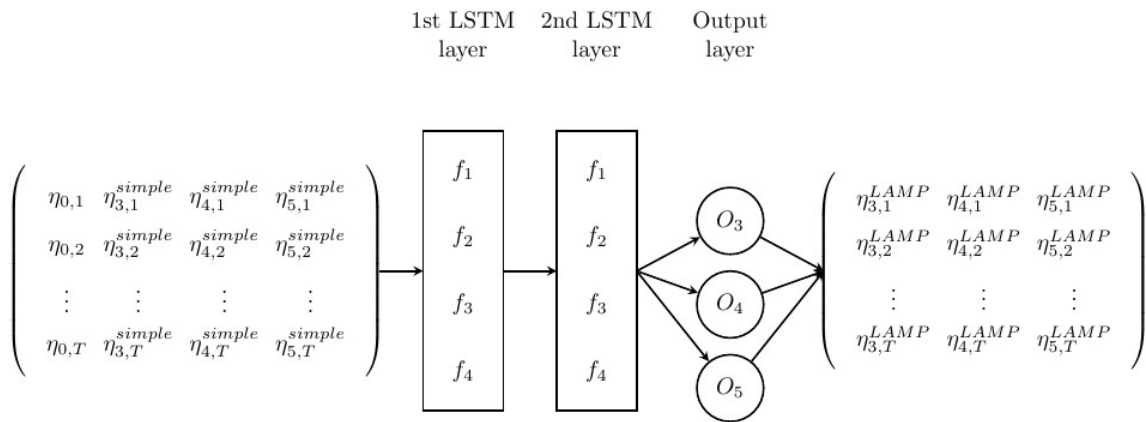


**Figure 6:** LSTM-SimpleCode Architecture

For training each of the neural networks, the maximum number of training epochs was set to 200. The training was considered complete once the maximum number of epochs was achieved, or if the mean-squared error of the training data did not improve by at least 1 percent over a set of epochs. For the 30 LAMP simulations, 15 were used as targets for training, and 15 for testing. After training had been completed, the test realizations were for providing an unbiased evaluation of the model fit.

The performance of each LSTM network was assessed in terms of the predicted standard deviations of the respective motion responses (heave, roll, and pitch) for each speed-heading combination. For each speed-heading combination, 100 realizations of 3-DOF ship motion response time-series were generated by SimpleCode.

As applicable, these ensembles were provided as inputs to the LSTM networks for the generation of the output realizations. For each speed-heading pairing and degree-of-freedom, the average standard deviation from these LSTM realizations was compared with the average standard deviation of the 30 realizations from LAMP as part of training phase. An individual LSTM network was trained for one speed-heading combination. This resulted in a total 91 LSTM networks corresponding to the 91 speed-heading combinations

After completion of the training, ensembles of motion time-series were generated by LAMP and SimpleCode. An ensemble was generated for each 3-DOF motion type (heave, roll, and pitch) at each speed-heading combination. The average standard deviation was estimated for each ensemble, which provided the ship motion response statistics for this study.

Irregular unidirectional waves were generated based on the Longuet-Higgins model using a Bretschneider spectrum with significant wave height ( $H_s$ ) of 4.0 m, and modal period ( $T_m$ ) of 15.0 seconds.

The hyperparameters were tuned using results from both head seas and beam seas configurations through a grid-search approach. Neither bi-directionality nor dropout were used due to increased computational expense and negligible gain in performance.

The training values for the hyperparameters are shown in Table 3.

**Table 3:** Training Values for Hyperparameters

Hyperparameter	Value
Length of Training Data Sequences	18,000
Time Resolution Factor	9
Hidden State Size	30
Number of LSTM Layers	2

## 4. RESULTS

This section presents the results of the comparative analysis of the ship motion statistics for LAMP, SimpleCode, LSTM-Waves, and LSTM-SimpleCode methods in terms of ship motion response plots and quantitative performance. As an illustrative example of seakeeping guidance, speed-heading polar plots of the 3-DOF ship motion responses from the LSTM-SimpleCode method are also provided.

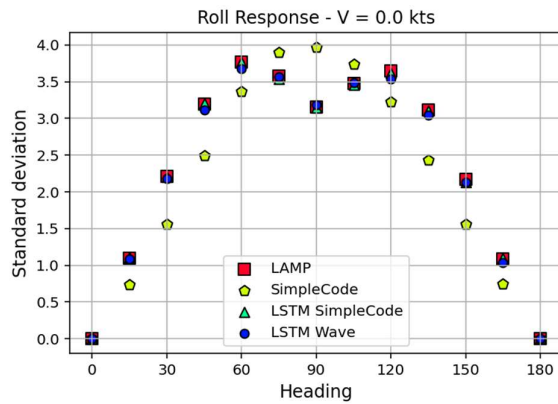
For these comparisons, the standard deviation of the ship motion response from LAMP serves as the higher-fidelity target. Based on the 30 realizations from LAMP, the average standard deviation of the ensemble provides an estimate of the true standard deviation (Belenky, et al., 2015).

### 4.1 Response Plot Comparisons

Response plot comparisons are rendered in two ways. In the first view, response levels are plotted versus heading for roll, pitch and heave. Responses are provided for LAMP, SimpleCode, LSTM-Waves and LSTM-SimpleCode at speeds of 0, 10, 20 and 30 knots in Figures 7, 8, 9, and 10, respectively. The heading convention for these and subsequent plots are head seas at 0 degrees, following seas at 180 degrees, and beam seas at 90 and 270 degrees.

In the second view, response trend-line comparisons are plotted relative to the LAMP target (vertical axis) versus corresponding estimates for SimpleCode, LSTM-Waves, and LSTM-SimpleCode on the horizontal axis, which are shown in Figures 11, 12, 13, and 14.

Responses at Speed = 0 knots



Responses at Speed = 10 knots

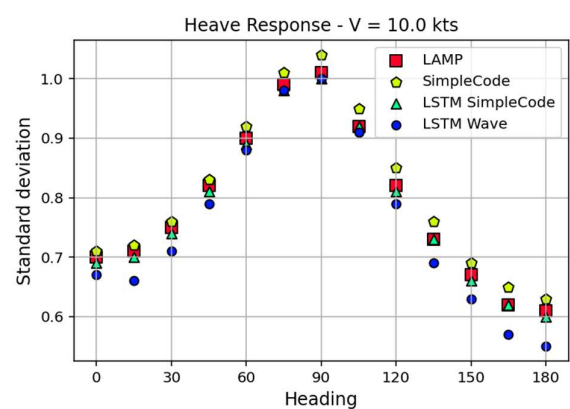
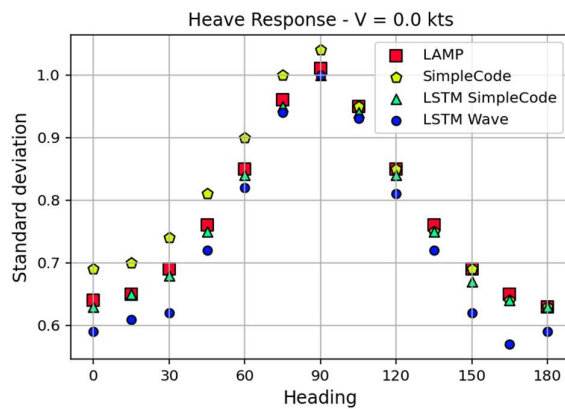
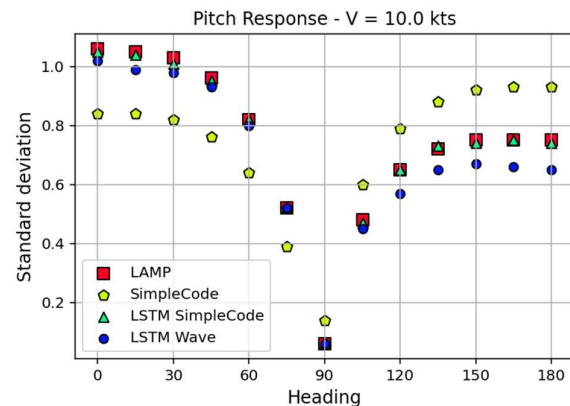
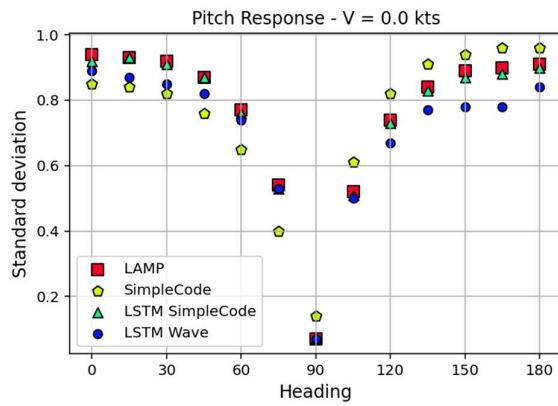
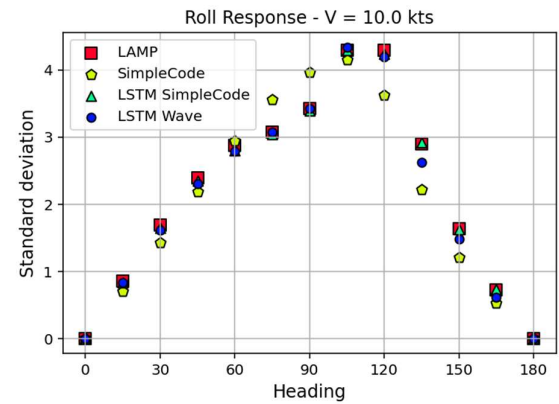


**Figure 7:** Comparison of response levels versus heading for roll (top plot), pitch (middle), and heave (bottom) at speed = 0 knots.

**Figure 8:** Comparison of response levels versus heading for roll (top plot), pitch (middle), and heave (bottom) at speed = 10 knots.

Responses at Speed = 20 knots

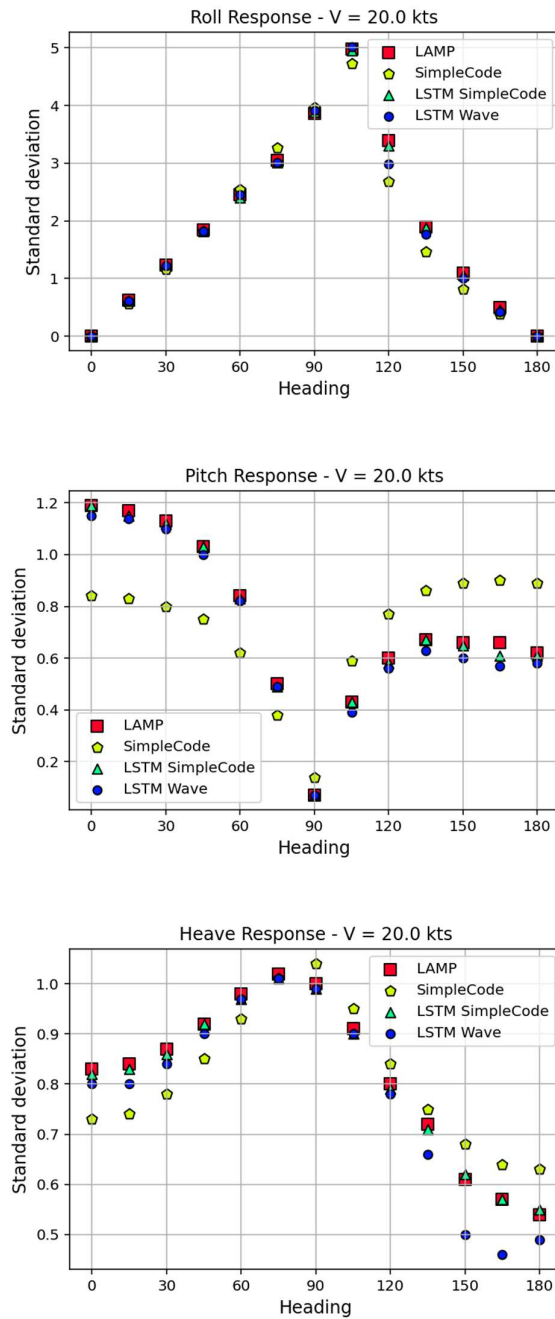


**Figure 9:** Comparison of response levels versus heading for roll (top plot), pitch (middle), and heave (bottom) at speed = 20 knots.

Responses at Speed = 30 knots

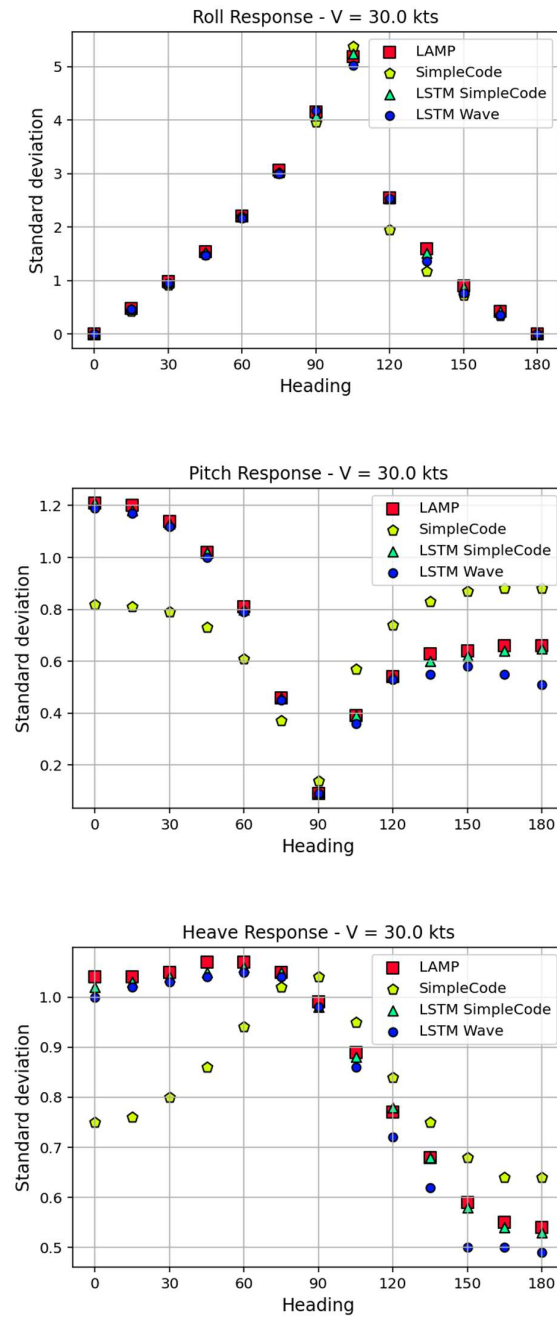
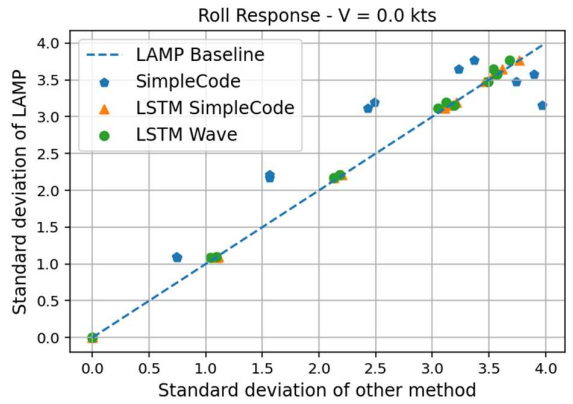


**Figure 10:** Comparison of response levels versus heading for roll (top plot), pitch (middle), and heave (bottom) at speed = 30 knots.

Responses at Speed = 0 knots



Responses at Speed = 10 knots

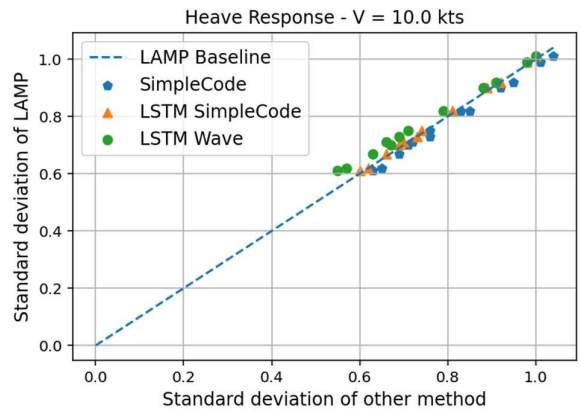
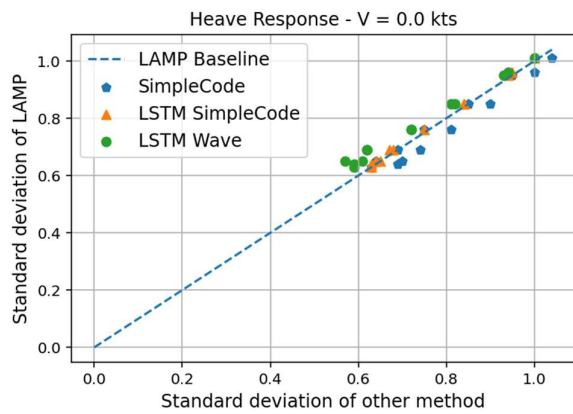
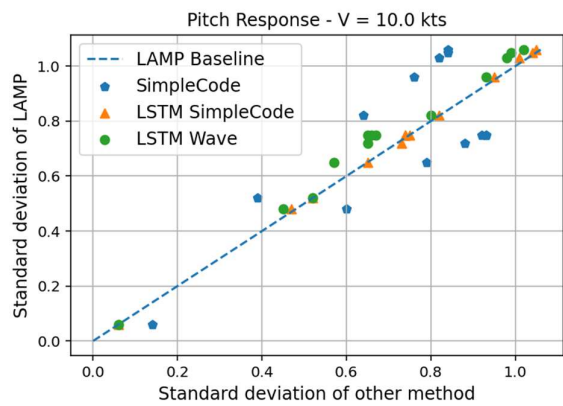
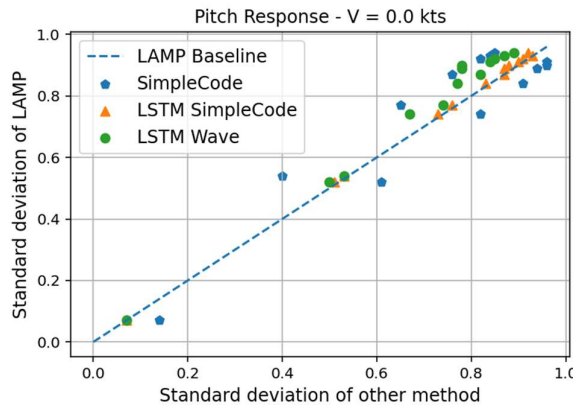
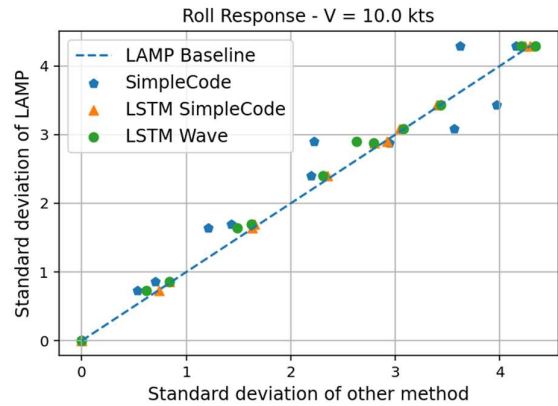


**Figure 11:** Comparison of response levels versus LAMP baseline for roll (top plot), pitch (middle), and heave (bottom) at speed = 0 knots.

**Figure 12:** Comparison of response levels versus LAMP baseline for roll (top plot), pitch (middle), and heave (bottom) at speed = 10 knots.

Responses at Speed = 20 knots

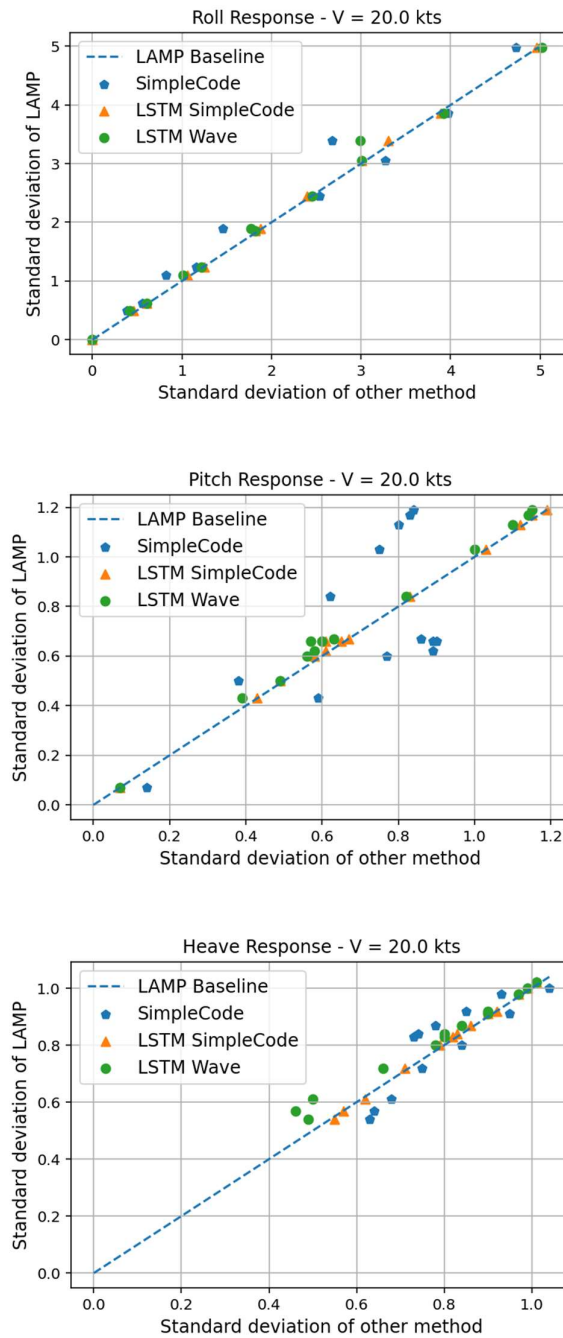


**Figure 13:** Comparison of response levels versus LAMP baseline for roll (top plot), pitch (middle), and heave (bottom) at speed = 20 knots.

Responses at Speed = 30 knots

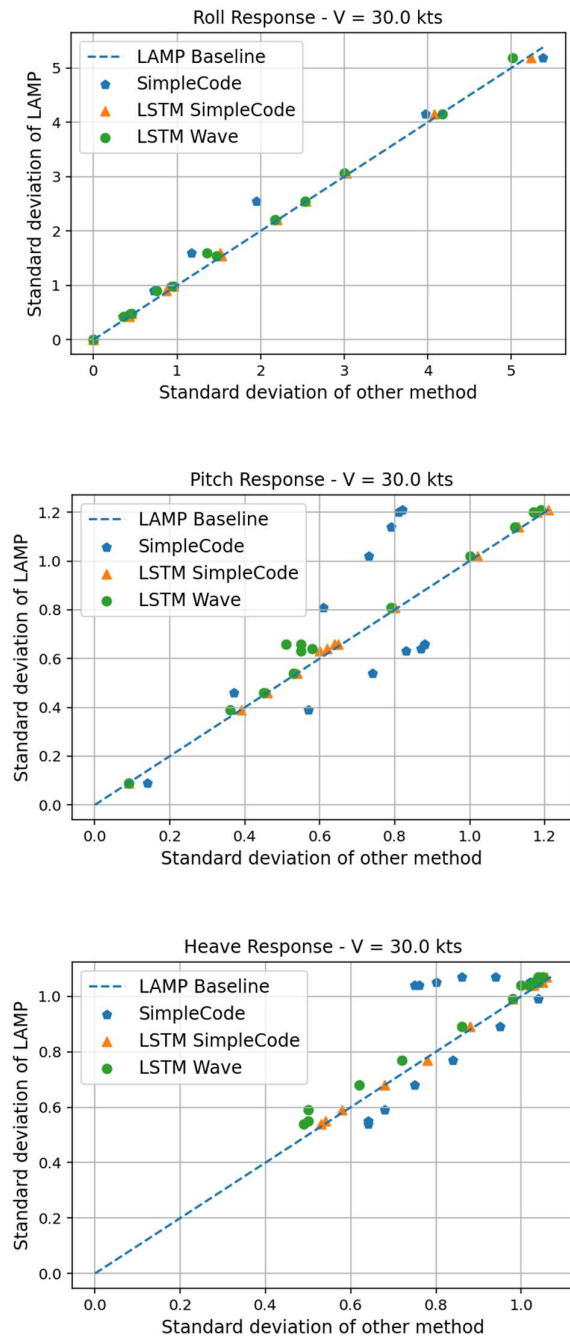


**Figure 14:** Comparison of response levels versus LAMP baseline for roll (top plot), pitch (middle), and heave (bottom) at speed = 30 knots.

## 4.2 Metric Based Comparison

As a quantitative metric for this assessment,  $R^2$  scores for SimpleCode, LSTM-Waves, and LSTM-SimpleCode are computed with respect to the LAMP baseline at each speed across headings.  $R^2$  is given as:

$$R^2 = 1.0 - \frac{MSE}{\sigma^2_{LAMP}} \quad (16)$$

$\sigma^2_{LAMP}$  is the variance of the LAMP standard deviations, and  $MSE$  is defined in Equation (15). Resultant  $R^2$  scores are shown in Table 3.

**Table 3:  $R^2$  Scores Comparison**

Motion	(kts)	SimpleCode	LSTM-SimpleCode	LSTM-Waves
	Speed			
Heave	0.0	0.9299	0.9935	0.8685
	10.0	0.9697	0.9953	0.9217
	20.0	0.8116	0.9965	0.8890
	30.0	0.4052	0.9969	0.9566
Roll	0.0	0.8599	0.9998	0.9983
	10.0	0.9306	0.9994	0.9947
	20.0	0.9682	0.9994	0.9932
Pitch	0.0	0.9786	0.9994	0.9961
	0.0	0.8591	0.9975	0.9249
	10.0	0.5829	0.9988	0.9506
	20.0	0.4043	0.9970	0.9822
	30.0	0.3997	0.9983	0.9649

Based on this comparisons, the LSTM-SimpleCode estimate most closely matched the LAMP target for all 3-DOF motions, headings, and speeds. In all cases, LSTM-SimpleCode  $R^2$  values exceeded 0.99, and outperformed LSTM-Waves and SimpleCode. LSTM-Waves estimates closely matched the LAMP target for roll, but showed some differences for heave and pitch. SimpleCode had the lowest  $R^2$  values particularly for pitch and heave at higher speeds.

## 4.3 Speed-Heading Polar Plots

For seakeeping guidance, speed-heading polar plots are typically used for visualizing ship motion responses for a given wave condition. Response levels are often provided as single significant amplitudes (SSA) in seakeeping studies (Levine et al, 2021). SSA is defined as an estimate of the largest one-third of observed amplitudes of motion. If the process is Gaussian, the estimate of the SSA is function of the estimated variance where:

$$\widehat{SSA} = 2 \cdot \sqrt{\widehat{V}_x} \quad (17)$$

To illustrate, Figure 15 shows the speed-heading polar plots for the 3-DOF ship motion responses predicted by the LSTM-SimpleCode method for the Sea State 5 condition in this study.

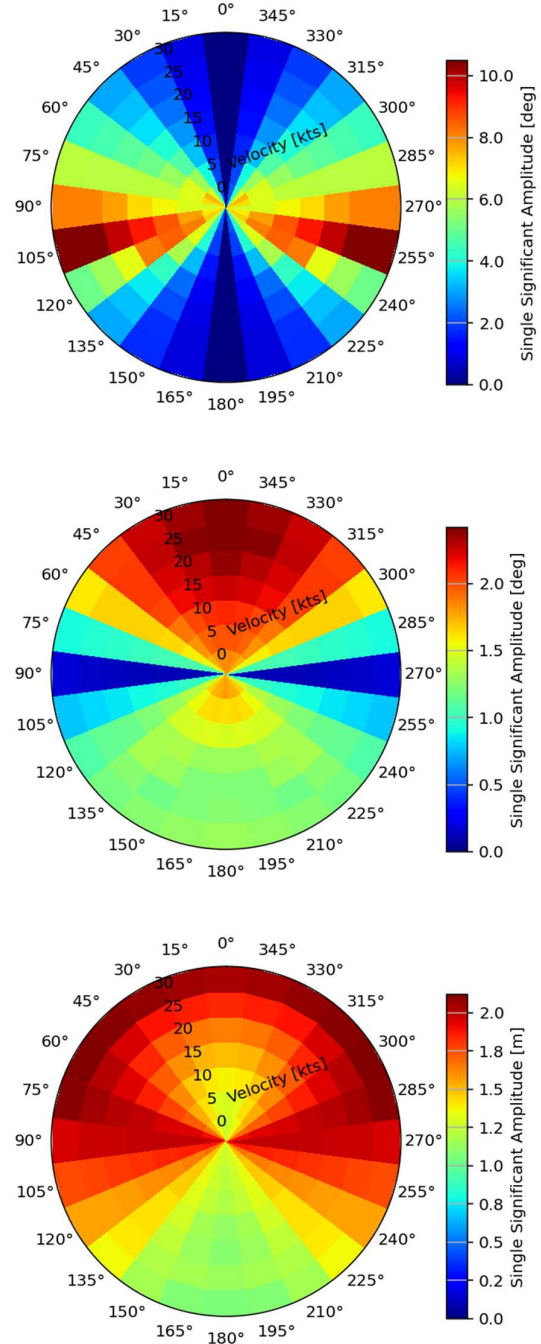


**Figure 15:** Speed-heading SSA response polar plots from LSTM-SimpleCode method for roll (top plot), pitch (middle), and heave (bottom).

The plots are rendered from 0 to 360 degrees; although, responses were only computed between 0 to 180 degrees. Since this case involved a symmetrical hull in unidirectional seas, response has been mirrored.

From the polar plots, speeds and headings with largest motion response can be readily identified by a human operator or automated detector. For this condition, the plots show the largest motion response for roll is around 105 degrees, pitch at 0 degrees, and heave at 75 degrees. Generally, response levels at these headings are greater at higher speeds.

## 5. CONCLUSIONS

An objective of this study has to been to assess the potential feasibility of a data-adaptive multi-fidelity model for autonomous seakeeping. In this study, data-adaptive tuning (or correction) of reduced-order model predictions have been implemented based on training with higher fidelity ship motion response data. From these initial results, this approach may provide a plausible means for improving the performance of a fast reduced-order model.

LSTM neural networks have been considered as part of a multi-fidelity approach for prediction of 3-DOF ship motion responses in waves. LSTM networks were trained and tested using LAMP simulations as a target, and SimpleCode simulations and wave time-series as inputs. LSTM networks were shown to improve the fidelity of SimpleCode seakeeping predictions relative to LAMP while retaining the computational efficiency of a reduced-order model.

LSTM-SimpleCode has been developed as a hybrid approach comprised of a physics-based model and data-adaptive stage. As a physics-based data-adaptive approach LSTM-SimpleCode most closely matched the LAMP target for all 3-DOF motions, the headings, and speeds. In all cases, the LSTM-SimpleCode outperformed the strictly data-driven LSTM-Waves approach. Based on the results of this study, LSTM-SimpleCode appears to be a suitable candidate for further investigation and application.

Potential future work includes:

- Application and investigation of this multi-fidelity approach with LSTM neural networks for automated guidance in terms of prediction of 6-DOF motions, structural loads, accelerations, and resistance.
- Further investigation of extreme response predictions.

- Extending assessment to cover a range of wave parameters in terms of significant wave heights and modal periods, as well as bimodal wave spectra.
- Application to other hull form geometries.
- Evaluation of LSTM network configurations in terms of hyperparameters and prediction performance.
- Application to autonomous path planning and weather routing.
- Verification and validation techniques for automated guidance algorithms and software.

## 6. ACKNOWLEDGEMENTS

The work described in this paper has been partially funded by the Office of Naval Research (ONR) under Dr. Woei-Min Lin.

Dayne Howard's graduate thesis work supporting this paper has been funded by the Department of the Navy as part of his enrollment in the Naval Construction and Engineering graduate program (Course 2N) at Massachusetts Institute of Technology.

## 7. REFERENCES

- ABS, 2019, "Guide for the Assessment of Parametric Roll Resonance in the Design of Container Carriers," American Bureau of Shipping, Houston, Texas, USA.
- Beck, R, and Reed, A., "Modern Computational Methods for Ships in Seaway," SNAME Transactions, Vol. 109, 2001, pp. 1-51.
- Belenky, V. L., "On Self-Repeating Effect in Reconstruction of Irregular Waves," Chapter 33 of Contemporary Ideas on Ship Stability, Neves, M. A. S., Belenky, V., de Kat, J.O., Spyrou, K. and N. Umeda, eds., Springer, ISBN 978-94-007-1481-6, 2011, pp. 589-598.
- Belenky, V., Yu, H., and Weems, K. M., "Numerical Procedures and Practical Experience of Assessment of Parametric Roll of Container Carriers," Chapter 16 of Contemporary Ideas on Ship Stability, Neves, M. A. S., Belenky, V., de Kat, J. O., Spyrou, K., and Umeda, N., eds., Springer, ISBN 978-94-007-1481-6, 2011, pp. 295-396.

- Belenky, V., Pipiras, V., and Weems, K., "Procedure for Probabilistic Evaluation of Large Amplitude Roll Motions," Proceedings of the 12<sup>th</sup> International Conference on the Stability of Ships and Ocean Vehicles, 2015, Glasgow, UK.
- Belknap, W., and Reed, A., "TEMPEST—A New Computationally Efficient Dynamic Stability Prediction Tool", Contemporary Ideas on Ship Stability. Risk of Capsizing, Springer International Publishing, 2019, pp. 3–21.
- Bertram, V., Practical Ship Hydrodynamics, 2<sup>nd</sup> edition, Butterworth-Heinemann ISBN 978-0080971506, 2011.
- Bickel, P. J., and Doksum, K. A., Mathematical Statistics: Basic Ideas and Selected Topics, Vol. 1. Person Prentice Hall, 2001.
- Bishop, R. C., Belknap, W., Turner, C., Simon, B., and Kim, J. H., "Parametric Investigation on the Influence of GM, Roll Damping, and Above-Water Form on the Roll Response of Model 5613", Report NSWCCD-50-TR-2005/027, 2005.
- France, W. M, Levadou, M., Treakle, T. W., Paulling, J. R., Michel, K. and Moore, C., "An Investigation of Head-Sea Parametric Rolling and its Influence on Container Lashing Systems," Marine Technology, Vol. 40, No. 1, 2003, pp. 1–19.
- Guth, S., and Sapsis. T., "Stochastically Precluded Wavegroups for Efficient Statistical Characterization of Systems Subjected to Random Waves," Proceedings of the 1<sup>st</sup> International Conference on the Stability and Safety of Ships and Ocean Vehicles, 2021, Glasgow, UK.
- Hochreiter, S., and Schmidhuber, J., "Long Short-Term Memory, Neural Computation, Vol. 9, No. 11, 1997, pp. 1735–1780,
- IACS, "Recommendation No. 34 Standard Wave Data," International Association of Classification Societies Recommendation, 2001, London, UK.
- IMO, "Interim Guidelines on the Second Generation Intact Stability Criteria," MCS.1/Circ. 1627, International Maritime Organization, 2020, London, UK.
- IMO, "Revised Guidance to the Master for Avoiding Dangerous Situations in Adverse Weather and Sea Conditions," MCS.1/Circ. 1228, International Maritime Organization, 2007, London, UK.
- IMO, "Guidance to the Master for Avoiding Dangerous Situations in Following and Quartering Seas", MSC/Circ. 707, International Maritime Organization, 1995, London, UK.
- ITTC, "Estimation of Roll Damping," Recommended Procedure 7.5-02-07-04.5, 29<sup>th</sup> International Towing Tank Conference, 2021.
- Levadou, M., and van't Veer, R., "Parametric Roll and Ship Design," Proceedings of the 9<sup>th</sup> International Conference on Stability of Ships and Ocean Vehicles (STAB 2006), Rio-de-Janeiro, Brazil, Vol. 1, 2006, pp. 191–206.
- Levine, M. D., Belenky, V., and Weems, K. M., "Method for Automated Safe Seakeeping Guidance," Proceedings of the 1<sup>st</sup> International Conference on the Stability and Safety of Ships and Ocean Vehicles, 2021, Glasgow, UK.
- Levine, M. D., Belenky, V., and Weems, K., "Statistical Uncertainty Techniques for Analysis of Simulation and Model Test Data," 30<sup>th</sup> American Towing Tank Conference, Naval Surface Warfare Center, Carderock Division, 2017, West Bethesda, MD, USA.
- Lin, W., and Yue, D., "Numerical Solutions for Large Amplitude Ship Motions in the Time-Domain," Proceedings of the 18<sup>th</sup> Symposium on Naval Hydrodynamics, 1990, Ann Arbor, Michigan, USA.
- Longuet-Higgins, M. S., 1984, "Statistical Properties of Wave Groups in a Random Sea State," Philosophical Transactions of the Royal Society of London A: Mathematical, Physical and Engineering Sciences, Vol. 312, No.1521, pp. 219-250.
- Pipiras, P., Belenky, V., Weems, K., Brown, B., Frommer, A., and Ouimette, G., 2021, "Calibrating Multifidelity Ship Motion Codes through Regression," Proceedings of the 1st International Conference on the Stability and Safety of Ships and Ocean Vehicles, 2021, Glasgow, UK.

Pipiras, P., Howard, D., Belenky, V., Weems, K., and Sapsis, T., “Multi-Fidelity Uncertainty Quantification and Reduced-Order Modeling for Extreme Ship Motions and Loads”, Proceeding of the 34<sup>th</sup> Symposium of Naval Hydrodynamics, Washington, D.C., 2022.

Qiao, D., Li, P., Ma, G., Qi, X., Yan, J., Ning, D., and Li, B., “Realtime Prediction of Dynamic Mooring Lines Responses with LSTM Neural Network Model.” Ocean Engineering, Vol. 219, No. 1, 2021.

Shin, Y. S., Belenky, V., Lin, W. M., and Weems, K. M., “Nonlinear Time Domain Simulation Technology for Seakeeping and Wave-Load Analysis for Modern Ship Design,” SNAME Transactions, Vol. 111, 2003, pp. 557–578.

Shin, Y. S., Belenky, V. L., Paulling, J. R., Weems, K. M., and Lin, W. M., “Criteria for Parametric Roll of Large Containerships in Longitudinal Seas,” SNAME Transactions, Vol. 112, 2004, pp. 14-47.

Smith, T. C., “Validation Approach for Statistical Extrapolation,” Chapter 34 of Contemporary Ideas on Ship Stability. Risk of Capsizing, Belenky, V., Neves, M., Spyrou, K., Umeda, N., van Walree, F., eds., Springer, ISBN 978-3-030-00514-6, 2019, pp. 573-589.

Weems, K. M., and Wundrow, D., “Hybrid Models for the Fast Time-Domain Simulation of Stability Failures in Irregular Waves with Volume based Calculations for Froude-Krylov and Hydrostatic Forces,” Proceedings of the 13<sup>th</sup> International Ship Stability Workshop, 2013, Brest, France.

Weems, K., and V. Belenky, 2018, “Extended Fast Ship Motion Simulations for Stability Failures in Irregular Seas,” Proceedings of the 13<sup>th</sup> International on Stability of Ships and Ocean Vehicles, 2018, Kobe, Japan.

Weems, K., Belenky, V., Spyrou, K., Aram, S. and K. Silva, “Towards Numerical Estimation of Probability of Capsizing Caused by Broaching-to,” Proceeding of the 33<sup>rd</sup> Symposium of Naval Hydrodynamics, 2020, Osaka, Japan.

Xu, W., Maki, K. J., and Silva, K. M., “A Data-driven Model for Nonlinear Marine Dynamics,” Ocean Engineering, Vol. 236, No. 9, 2021.